

Depth-dependent charge collection profile of pad diodes

M. Hajheidari^{a,*}, E. Garutti^a, J. Schwandt^a, A. Ebrahimi^b

^a*Institute for Experimental Physics, University of Hamburg, Luruper Chaussee 149, 22761 Hamburg, Germany*

^b*Paul Scherrer Institut, Villigen, Switzerland*

Abstract

The collected charge of two pad diodes is measured along the diode width using a 5.2 GeV electron beam at the DESY II beam test facility. The electron beam enters parallel to the readout electrode plane and perpendicular to the edge of the diode. The position of the electron beam is reconstructed by three planes of an EUDET-type telescope. An in-situ procedure is developed to align the diode surface parallel to the electron beam. The result of these measurements is the charge collection efficiency profile as a function of depth for each diode. For a non-irradiated diode, the charge profile is uniform as a function of the beam position for bias voltages above the full-depletion, as expected. For the irradiated diode, the charge profile is non-uniform and changes as a function of bias voltage.

Keywords: Transient Current Technique, edge-on method, electron beam, irradiated silicon pad diode

1. Introduction

Transient Current Technique (TCT) is a well-known method to study irradiated silicon sensors. In one flavour of this technique so-called Top-TCT, the Device Under Test (DUT) is illuminated by α -particles [1, 2, 3] or red light and infra-red (IR) laser [4, 5, 6], and the induced current transient is recorded. One can determine the collected charge by integrating this transient. The result of this measurement is a quantity called "Charge Collection Efficiency" or CCE defined as the ratio between the collected charge by the electrodes and the produced charge inside the sensor.

Due to the short absorption depth of α -particles and red light in silicon, all electron-hole pairs are generated close to the surface of the diode. Therefore, only one of the charge carrier types (electrons or holes) is drifting through the bulk region while the other is collected immediately at the implant. The induced signal in the electrodes of the diode is dominated by the charge carrier type which is drifting through the entire bulk and the other type has a minor contribution to the signal. As a result, one can study the trapping times of electrons and holes separately using this technique for irradiated sensors. Using IR light, one can obtain the overall CCE of irradiated samples with contribution from both electrons and holes.

Top-TCT with alpha particle and red -light laser is limited for studying highly irradiated pad diodes. The estimated CCE values from these measurements are very sensitive to possible inactive layers in the sensor implants. There is a field-free region in the diode implant where the generated electron-hole pairs can be trapped before they diffuse to the active region of the diode (the region with a non-zero electric field) [7, 8]. Simulation of a non-irradiated diode shows that this region remains field-free

independent of the applied voltage. As a result, the measured CCE values with the Top-TCT method using alpha-particles or red light underestimate the actual CCE in the active region of irradiated diodes and are affected by the change of the thickness of the non-depleted layer, depending on the irradiation fluence.

In another flavour of this technique called "edge-TCT" or E-TCT, the sensor is illuminated by focussed IR laser light from the edge [9]. By scanning the light along the edge, one can obtain information on the charge collection as a function of depth. This method has been used to study strip sensors to extract their charge and electric field profiles [10, 11, 12]. An issue with this technique is that the waist radius of the light spot changes as it travels through the sensor and the beam becomes defocused. As a result, it can only be used for segmented sensors (strips and pixels) where the charge produced below a narrow strip is collected and read out. This technique cannot be used for measuring pad diodes where there is only one readout electrode. Another issue is that it is not straightforward to normalize E-TCT measured charges to an absolute value, as the exact number of electron-hole pairs generated by light in the sensor is not known. In addition, it has been shown that the absorption length of infrared light changes after irradiation [13]. Therefore, a direct comparison between irradiated and non-irradiated detectors is not straightforward.

This work uses an electron beam (5.2 GeV) for edge-on measurements on pad diodes. Charge collection profiles as a function of depth have been measured for pixel detector at grazing angles [14]. For pad diodes, the edge-on method was introduced in [15]. In that work, pions with an energy of 120 GeV were used to study 300 μm thick pad diodes. However, no results about the charge collection of the studied diode were shown in that paper. Moreover the required alignment accuracy was not discussed and no alignment procedure was presented. It should be noted that the alignment has to be performed on-line

*Corresponding author: mohammadtaghi.hajheidari@desy.de

so that the data are taken with the sensor aligned to the beam.

The main aim of this study is to obtain the position-dependent charge collection perpendicular to the electrode plane. The Charge Collection Distance (CCD), or the mean distance in which charge carriers drift inside the sensor before trapping, can be estimated using the results of these measurements. The advantages of this technique compared to the Edge-TCT with IR light are:

- Radius and direction of the beam do not change as it travels through the sensor. The estimated deflection angle of an electron beam with an energy of 5.2 GeV after traveling in 5.0 mm of silicon is 0.53 mrad [16]. This number is well within the uncertainty of the measurements. Therefore, the method can be used to study pad diodes.
- An absolute normalization is possible as the energy loss of the beam in the sensor, i.e. average dE/dx , is well known.
- The energy lost of the electron beam by charge deposition does not change after irradiation. Therefore, one can directly compare the results of the non-irradiated and irradiated diodes together.

The disadvantages of this technique are:

- Due to the large capacitance of pad diodes, rise times of induced signals on the electrodes are in a order of a few nanoseconds. As a result, it is not straightforward to extract information about charge carrier velocity and electric field from the transients.
- The alignment procedure proposed in this paper is limited for highly irradiated sensors where the charge collection profile is not uniform as a function of depth.

The paper is structured in the following way. After introducing the experimental setup, an in-situ alignment is proposed to find the minimal angle between the electron beam and the diode surface. In the result section, the collected charge profile for the no-irradiated is shown for different bias voltages and beam energies. In addition, the collected charge profile of an irradiated diode is shown as a function bias voltage.

2. Experiment Setup

The measurements are performed in at Deutsches Elektronen-Synchrotron (DESY) test beam facility. In this facility, electron/positron beams with energy in a range of 1 – 6 GeV are available [17]. For this work, the electron beam with an energy of 5.2 GeV is chosen. A schematic view of the setup used for these measurements is shown in Fig. 1.

The tracks are reconstructed using three planes of an EUDET-type telescope. Each plane of the telescope consists of a MIMOSA 26 sensor [18]. This is a monolithic pixel sensor produced in 350 nm CMOS technology. The pixel size is $18.4 \times 18.4 \mu\text{m}^2$ and the thickness of the sensor is $54.5 \pm 3.6 \mu\text{m}$. Each sensor contains 1152 columns and 576 rows which cover

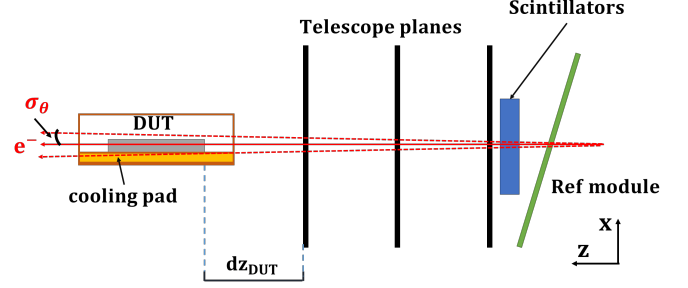


Figure 1: Schematic view of the beam test setup used for edge-on measurements. In this sketch, DUT (the Device Under the Test) is the pad diode, Ref module is the timing reference module, Scintillators provide the readout trigger, and Telescope planes reconstruct the tracks. The divergence of the electron beam is shown with two dash lines (σ_θ). The distance between the third plane of the telescope and the DUT is shown with dz_{dut} .

an area of $21.2 \times 10.6 \text{ mm}^2$. The readout of the sensors is binary. The estimated intrinsic hit resolution of a single plane is $3.24 \pm 0.9 \mu\text{m}$ [19]. The threshold of the telescope sensors is set to 4 mV corresponding to $\sim 70 e^-$.

The integration time of the MIMOSA 26 planes is relatively long (115 μs). Therefore, a time reference is needed to select a subset of tracks that are contained in one readout cycle. The time reference is provided by a CMS phase 1 pixel module. This module contains a silicon sensor with a pixel size of $100 \times 150 \mu\text{m}^2$ and a PSI46dig readout chip. The internal clock of the readout chip is 40 MHz (correspond to 25 ns readout cycle).

The trigger signal for readout of the telescope, timing reference module, and DUT is provided by two orthogonally mounted scintillators coupled to Photo Multiplier Tubes (PMTs). The scintillators are placed in front of the telescope planes. The coincidence signal between them provides a triggering area of $8 \times 3 \text{ mm}^2$. The output of the PMTs is fed to a device called Trigger Logic Unit (TLU) [20]. The TLU provides the trigger signal through a logic AND between signals of two scintillators.

The diodes in this work are p -type (n^+pp^+ configuration) with an active thickness of 150 μm . The active area of diodes is $\approx 25 \text{ mm}^2$. Fig. 2 show the top view of the studied diodes. One diode is irradiated with 23 MeV protons to a 1 MeV neutron equivalent fluence Φ_{eq} of $2 \times 10^{15} \text{ cm}^{-2}$. For the calculation of Φ_{eq} , a hardness factor $\kappa = 2.2$ is used [21]. From the capacitance-voltage measurement, the depletion voltage of the non-irradiated diode is determined to be around 75 V and the doping density of the bulk region $4.5 \times 10^{12} \text{ cm}^{-3}$. The guard ring of the diodes is floating during the measurement.

A Rohde & Schwarz oscilloscope with an analog bandwidth of 4 GHz and a sampling rate of 20 GS/s records the transients. A Femto HSA-X-40 amplifier with a bandwidth of 2.0 GHz and a nominal gain of 100 amplifies the transient [22]. The trigger is provided externally through the TLU. The external triggering makes it possible to record all transients without zero suppression.

To calculate the collected charge, transients are integrated in

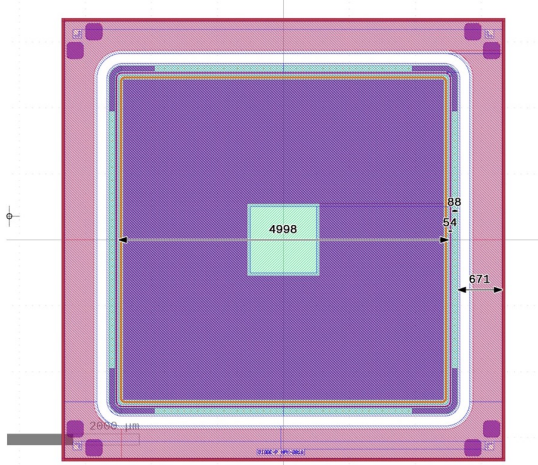


Figure 2: Top view of the diode (dimensions in μm).

a time window (gate). The charge is calculated as:

$$Q = \int_{t_0}^{t_1} \frac{U(t)}{G \cdot R_L} dt \quad (1)$$

$U(t)$ is the transient after the baseline correction and R_L is the input impedance of the oscilloscope (50Ω) and G is the nominal gain of the amplifier (100). For this study, a gate width of 30 ns is chosen.

To measure the transients, the diode is mounted on a PCB which provides the electrical connectors. The parallel beam can produce showers inside the PCB. These showers can produce particles which deposit energy in the DUT. To cancel the effects of these showers on the response of the diode, two spacers are inserted between the diode and the PCB. These spacer are metal bars with a width of $w = 1 \text{ mm}$ and a thickness of $d = 0.5 \text{ mm}$.

3. Online alignment

The method proposed in this paper only works if tracks are parallel to the diode surface. To ensure this condition, an "on-line alignment" procedure is used before data taking. It is important to point out that this procedure has to be done online and before one can start taking data and cannot be corrected offline.

In this procedure, the mean collected charge is measured as a function of angle with fine steps (0.1° or $\approx 1.7 \text{ mrad}$). The minimum step size of the rotation stage is 0.01° . The minimum or "zero" angle is defined as the angle where the measured charge is maximum. If tracks and diode surface are not parallel, a part of the tracks leaves the diode through the top or bottom plane and therefore deposit less charge than tracks that cross the whole diode (5 mm). As a result, the average charge is maximal when the angle between the tracks and the diode is minimal. The important assumption in this procedure is that the collected charge is uniform as a function of depth.

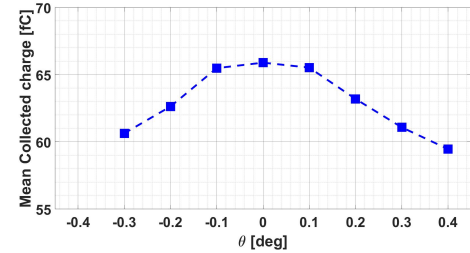
The uncertainty of the position reconstruction due to the angular spread of the beam (σ_θ) is given by $d \cdot \sigma_\theta$, where d is the length of the diode which is 5 mm for this study. This quantity

should be kept smaller than the resolution $\sigma_{x,beam}$. The uncertainty due to the step size of the angle scan ($\Delta\theta$), which is given by $d \cdot \Delta\theta$, should be smaller than the resolution $\sigma_{x,beam}$ as well.

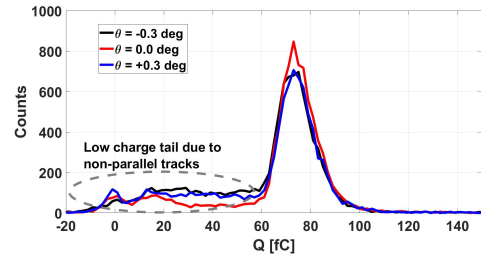
In [18], the telescope resolution was calculated as a function of the DUT-to-telescope distance (i.e. $d_{z,DUT}$ in Fig. 1). By assuming a resolution around $10 \mu\text{m}$, the maximum value for σ_θ and $\Delta\theta$ is estimated to be 2.0 mrad . In the offline analysis, a cut is applied on the slope of reconstructed track to select the ones with a slope less than $\pm 1.0 \text{ mrad}$. The step size of the angle scan is chosen 0.10° or 1.7 mrad .

Fig. 3a shows the average collected charge of the non-irradiated diode as a function of angle (θ). The measurement is done at a bias voltage of 120 V and at room temperature. For each angle, 20,000 triggers are collected. To obtain this plot, an offline threshold of 20 mV is applied to the recorded transients. Fig. 3b shows the charge distributions for three angles. One can notice, for non-zero angles, the charge distributions show a tail below the peak around 75 fC towards the lower charges. This tail corresponds to the tracks which partially crossed the diode and it is minimal when θ is minimal.

The procedure exploits a simple geometrical relation between the track length inside the DUT and the angle of incidence. The advantage of using this procedure is that no track reconstruction was required. This procedure had to be repeated once the diode is changed or the cooling box is dismantled.



(a) Mean collected charge as a function of the angle (θ) for the non-irradiated diode. The plot is obtained for transients with amplitude higher than 20 mV.



(b) Collected charge distribution at three angles for non-irradiated diode.

Figure 3: Results of the online alignment procedure needed to adjust the angle of the diode w.r.t. the beam before starting data taking. As a result of the scan, the angle for which the mean collected charge is maximum is defined to be $\theta = 0^\circ$.

4. Results for the non-irradiated diode

After finding the minimum angle, the final data is taken. The beam tracks are reconstructed and projected to the surface of the

diode facing the beam. To gain maximum acceptance, the centering of the diode with respect to the trigger area is checked.

Fig. 4 shows the charge profile as a function of depth for the non-irradiated diode at a bias voltage of 120 V and at room temperature. For comparison, the measurement is repeated at a lower beam energy of 4.2 GeV and different diode-to-telescope distance (dz_{dut}). One can see by increasing E_{beam} and decreasing dz_{dut} , the profile at the edges become sharper and the spatial resolution of the measurement improves.

Fig. 5 shows the charge distribution for bins with $-10 \mu\text{m} < x < +10 \mu\text{m}$. Using a GEANT4 simulation, the mean deposition energy of 5.0 GeV electron beam in 5 mm of silicon is estimated to be 1.767 MeV. One can convert the deposited energy to the deposited charge by taking into account the ionisation energy of silicon, 3.64 eV and the elementary charge:

$$Q_{\text{deposit}} = E_{\text{deposit}} \cdot \frac{1.6 \times 10^{-19} \text{ C}}{3.64 \text{ eV}} = 77.6 \text{ fC}$$

This value is in a good agreement with the measured absolute charge shown in Fig. 5.

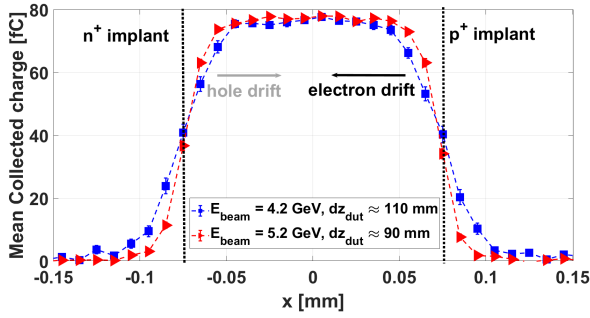


Figure 4: Charge profile of the non-irradiated diode at bias voltage of 120 V.

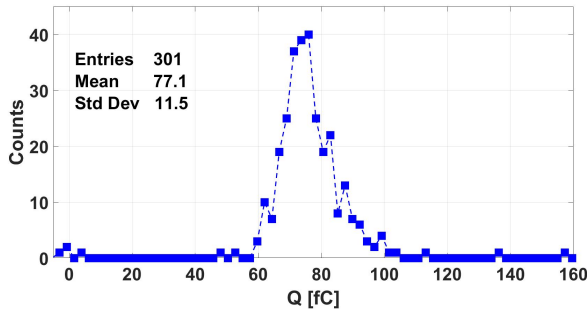


Figure 5: The charge distribution for a central bin with $-10 \mu\text{m} < x < +10 \mu\text{m}$.

The measurements are repeated for bias voltages in the range of 20 – 120 V. Fig. 6 shows the charge profiles obtained from these measurements. One can see that for bias voltage above 80 V, the profile remains unchanged. At bias voltage of 40 V and 20 V, the charge collection is zero in the region near the p^+ implant. This can be explained by the fact that the electric field expands from the n^+ to the p^+ implant. At bias voltages below

the full depletion voltage, 75 V, the electric field is zero near the p^+ region and results in a region with zero charge collection.

One can estimate the active thickness of the diode from the profiles shown in Fig. 6 by fitting the following function to the data:

$$F(x) = A \cdot \int_x^{x+dx} \left(\text{erf}\left[\frac{x' - \mu_1}{\sqrt{2}\sigma}\right] - \text{erf}\left[\frac{x' - \mu_2}{\sqrt{2}\sigma}\right] \right) dx' \quad (2)$$

The active thickness is estimated as $\mu_2 - \mu_1$.

For bias voltages of 40 V and 20 V, the active thickness is estimated to be 115 μm and 83 μm , respectively. The depletion depth of the diode at a bias voltage of V_{bias} can be calculated using the following equation:

$$d = \sqrt{\frac{2\epsilon_s\epsilon_0 V_{bias}}{eN_A}} \quad (3)$$

where e is the elementary charge, ϵ_0 the vacuum permittivity ($8.85 \times 10^{-12} \text{ F} \cdot \text{m}^{-1}$), ϵ_s the relative permittivity of silicon (11.7) and N_A the doping concentration of bulk region ($4.5 \times 10^{12} \text{ cm}^{-3}$). The calculated depletion depth from Eq. (3) at bias voltages of 40 V and 20 V is 107 μm and 76 μm , respectively. Compared to the estimated active thickness from the measurements, the calculated depletion depths are slightly lower. This can be explained by taking into account the effect of the diffusion of charge carriers from non-depleted region to the active region. Due to this effect, the thickness of the region with non-zero charge collection is slightly larger than the depletion depth.

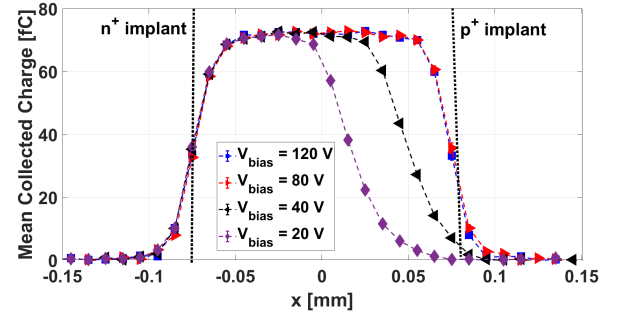


Figure 6: Charge collection profiles of non-irradiated diode at few bias voltages.

5. Results for irradiated diodes

The measurements explained in Sections 3 and 4 are repeated for an irradiated diode. In order to keep the leakage current of the diode low, it is mounted in a cold box. The box is cooled down using a circulation chiller (operating at -20°C) and two Peltier elements. The exact temperature inside the box is not measured. Fig. 7 show the charge profiles for the irradiated diode at $\Phi_{eq} = 2 \times 10^{15} \text{ cm}^{-2}$ at different bias voltages, along with the charge profile of the non-irradiated diode at the bias voltage of 120 V.

From these figures, one can see that the charge profile is not uniform as a function of depth, especially at low bias voltages.

For both diodes, the collected charge near the n^+ implant, which is dominated by holes, is higher than at the p^+ implant. These results are in agreement with previously published results on velocity and electric field profiles of irradiated strip sensors [23, 12]. In these references, one can see high electric fields near n^+p and pp^+ implants and a lower electric field in the center of the sensor. Moreover, one can see a more uniform electric field at high bias voltages which is in agreement with the measured collected charge profile presented in this paper. At the highest bias voltage, a reduced CCE is seen which is a consequence of trapping of charge carriers.

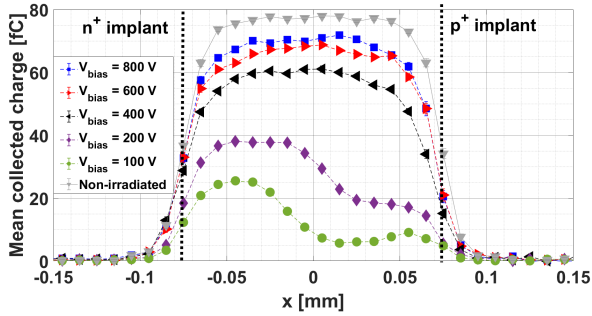


Figure 7: Charge collection profiles of non-irradiated diode at bias voltage of 120 V and irradiated diode ($\Phi_{eq} = 2 \times 10^{15} \text{ cm}^{-2}$) at several bias voltages.

6. Conclusion

In this paper, we demonstrate the feasibility of using an electron beam entering the side of a silicon pad diode to obtain the depth-dependence charge collection efficiency profile. We introduce an online method to find the minimum angle between the diode and electron beam.

It is shown that the charge collection profile of a non-irradiated pad diode is uniform as a function of depth for bias voltages above full depletion. The profile of irradiated diode, however, is not uniform, especially for lower bias voltages. For the highest applied bias voltage, 800 V, the CCE is less than 1 for the investigated irradiated diode.

Qualitatively, it is observed that the shape of measured charge collection profiles in this paper is in agreement with previously published measurements of the electric fields for irradiated strip sensors.

It was shown that the method can be further optimized. The resolution can be improved by minimizing the distance between the telescope and the DUT and increasing the beam energy. The efficiency of data selection can be improved by optimizing the geometrical match between the DUT and the trigger scintillator.

7. Acknowledgements

The authors acknowledge support by the BMBF, the German Federal Ministry of Education and Research. This work was funded by the Deutsche Forschungsgemeinschaft (DFG, German Research Foundation) under Germany's Excellence Strategy – EXC 2121 “Quantum Universe” – 390833306.

The measurements leading to these results has been performed at the Test Beam Facility at DESY Hamburg (Germany), a member of the Helmholtz Association (HGF).

References

- [1] G. Kramberger, V. Cindro, I. Mandić, M. Mikuž, M. Zavrtanik, Effective trapping time of electrons and holes in different silicon materials irradiated with neutrons, protons and pions, *Nucl. Instrum. Methods Phys. Res. A* (2002). doi:[https://doi.org/10.1016/S0168-9002\(01\)01263-3](https://doi.org/10.1016/S0168-9002(01)01263-3).
- [2] G. Kramberger, V. Cindro, I. Mandić, M. Mikuž, M. Zavrtanik, Determination of effective trapping times for electrons and holes in irradiated silicon, *Nucl. Instrum. Methods Phys. Res. A* (2002). doi:[https://doi.org/10.1016/S0168-9002\(01\)01653-9](https://doi.org/10.1016/S0168-9002(01)01653-9).
- [3] T. Brodbeck, A. Chilingarov, T. Sloan, E. Fretwurst, M. Kuhnke, G. Lindstroem, A new method of carrier trapping time measurement, *Nucl. Instrum. Methods Phys. Res. A* (2000). doi:[https://doi.org/10.1016/S0168-9002\(00\)00573-8](https://doi.org/10.1016/S0168-9002(00)00573-8).
- [4] H. Kraner, Z. Li, E. Fretwurst, The use of the signal current pulse shape to study the internal electric field profile and trapping effects in neutron damaged silicon detectors, *Nucl. Instrum. Methods Phys. Res. A* (1993). doi:[https://doi.org/10.1016/0168-9002\(93\)90376-S](https://doi.org/10.1016/0168-9002(93)90376-S).
- [5] L. Beattie, T. Brodbeck, A. Chilingarov, G. Hughes, S. McGarry, P. Ratoff, T. Sloan, Carrier lifetimes in heavily irradiated silicon diodes, *Nucl. Instrum. Methods Phys. Res. A* (1999). doi:[https://doi.org/10.1016/S0168-9002\(98\)01229-7](https://doi.org/10.1016/S0168-9002(98)01229-7).
- [6] J. Fink, H. Krueger, P. Lodomez, N. Wermes, Characterization of charge collection in cdte and czt using the transient current technique, *Nucl. Instrum. Methods Phys. Res. A* (2006). doi:<https://doi.org/10.1016/j.nima.2006.01.072>.
- [7] C. Scharf, R. Klanner, Measurement of the drift velocities of electrons and holes in high-ohmic $< 100 >$ silicon, *Nucl. Instrum. Methods Phys. Res. A* (2015). doi:<https://doi.org/10.1016/j.nima.2015.07.057>.
- [8] C. Scharf, Radiation damage of highly irradiated silicon sensors, Phd thesis (2018).
- [9] G. Kramberger, V. Cindro, I. Mandić, M. Mikuž, M. Milovanovic, M. Zavrtanik, K. Zagar, Investigation of Irradiated Silicon Detectors by Edge-TCT, *IEEE Trans. Nucl. Sci.* (2010). doi:<https://doi.org/10.1109/TNS.2010.2051957>.
- [10] I. Mandić, V. Cindro, A. Gorišek, G. Kramberger, M. Mikuž, M. Zavrtanik, Edge-tct measurements with the laser beam directed parallel to the strips, *Journal of Instrumentation* (2015). doi:[10.1088/1748-0221/10/08/P08004](https://doi.org/10.1088/1748-0221/10/08/P08004).
- [11] I. Mandić, V. Cindro, A. Gorišek, G. Kramberger, M. Mikuž, M. Milovanović, M. Zavrtanik, Tct measurements of irradiated strip detectors with a focused laser beam, *Journal of Instrumentation* (2013). doi:[10.1088/1748-0221/8/04/P04016](https://doi.org/10.1088/1748-0221/8/04/P04016).
- [12] R. Klanner, G. Kramberger, I. Mandić, M. Mikuž, M. Milovanović, J. Schwandt, Determination of the electric field in highly-irradiated silicon sensors using edge-tct measurements, *Nucl. Instrum. Methods Phys. Res. A* (2020). doi:<https://doi.org/10.1016/j.nima.2019.162987>.
- [13] C. Scharf, F. Feindt, R. Klanner, Influence of radiation damage on the absorption of near-infrared light in silicon, *Nucl. Instrum. Methods Phys. Res. A* (2020). doi:<https://doi.org/10.1016/j.nima.2020.163955>.
- [14] V. Chiochia, M. Swartz, D. Bortoletto, L. Cremaldi, S. Cucciarelli, A. Dorokhov, C. Hormann, D. Kim, M. Konecki, D. Kotlinski, et al., Simulation of heavily irradiated silicon pixel sensors and comparison with test beam measurements, *IEEE transactions on nuclear science* (2005). doi:[10.1109/TNS.2005.852748](https://doi.org/10.1109/TNS.2005.852748).
- [15] A. Gorišek, V. Cindro, G. Kramberger, I. Mandić, M. Mikuž, M. Muškinja, M. Zavrtanik, The edge transient-current technique (e-tct) with high energy hadron beam, *Nucl. Instrum. Methods Phys. Res. A* (2016). doi:<https://doi.org/10.1016/j.nima.2016.03.061>.
- [16] G. R. Lynch, O. I. Dahl, Approximations to multiple coulomb scattering, *Nuclear Instruments and Methods in Physics Research Section B: Beam Interactions with Materials and Atoms* 58 (1) (1991) 6–10.

- [17] R. Diener, J. Dreyling-Eschweiler, H. Ehrlichmann, I.-M. Gregor, U. Kötz, U. Krämer, N. Meyners, N. Potylitsina-Kube, A. Schütz, P. Schütze, et al., The DESY II test beam facility, *Nucl. Instrum. Methods Phys. Res. A* (2019). doi:<https://doi.org/10.1016/j.nima.2018.11.133>.
- [18] H. Jansen, S. Spannagel, J. Behr, A. Bulgheroni, G. Claus, E. Corrin, D. Cussans, J. Dreyling-Eschweiler, D. Eckstein, T. Eichhorn, et al., Performance of the eudet-type beam telescopes, *EPJ Techniques and Instrumentation* (2016). doi:[10.1140/epjti/s40485-016-0033-2](https://doi.org/10.1140/epjti/s40485-016-0033-2).
- [19] C. Hu-Guo, J. Baudot, G. Bertolone, A. Besson, A. Brogna, C. Colledani, G. Claus, R. De Masi, Y. Degerli, A. Dorokhov, et al., First reticule size maps with digital output and integrated zero suppression for the eudet-jral beam telescope, *Nucl. Instrum. Methods Phys. Res. A* (2010). doi:<https://doi.org/10.1016/j.nima.2010.03.043>.
- [20] D. Cussans, Description of the jral trigger logic unit (tlu), v0. 2c, EUDETMemo-2009-04 (2009).
- [21] P. Allport, F. Bögelspacher, K. Bruce, R. Canavan, A. Dierlamm, L. Gonella, P. Knights, I. Mateu, M. Moll, K. Nikolopoulos, et al., Experimental determination of proton hardness factors at several irradiation facilities, *Journal of Instrumentation* (2019). doi:[10.1088/1748-0221/14/12/P12004](https://doi.org/10.1088/1748-0221/14/12/P12004).
- [22] FEMTO Messtechnik GmbH, Klosterstrasse 64, 10179 Berlin, Germany, <http://www.femto.de/>, Accessed: 2021 (2021).
- [23] G. Kramberger, V. Cindro, I. Mandić, M. Mikuž, M. Milovanović, M. Zavrtnik, Modeling of electric field in silicon micro-strip detectors irradiated with neutrons and pions, *Journal of Instrumentation* (2014). doi:[10.1088/1748-0221/9/10/P10016](https://doi.org/10.1088/1748-0221/9/10/P10016).